The Role of Qiongzhou Strait in the Seasonal Variation of the South China Sea Circulation

MAOCHONG SHI

Department of Oceanography and Meteorology, Ocean University of Qingdao, Qingdao, China

CHANGSHENG CHEN

School for Marine Sciences and Technology, University of Massachusetts—Dartmouth, New Bedford, Massachusetts

QICHUN XU

Institute of Physical Oceanography, Ocean University of Qingdao, Qingdao, China

HUICHAN LIN

Department of Geophysics and Geology, Woods Hole Oceanographic Institution, Woods Hole, Massachusetts

GUIMEI LIU AND HUI WANG

The Institute of Oceanology, The Chinese Academy of Sciences, Qingdao, China

FANG WANG AND JINHUI YAN

The Center of Marine Survey Technology, The Branch Bureau of the South China Sea, SOA, Guangzhou, China

(Manuscript received 5 June 2000, in final form 3 May 2001)

ABSTRACT

An analysis of the water level and current data taken in Qiongzhou Strait in the South China Sea (SCS) over the last 37 years (1963 to 1999) was made to examine the characteristics of tidal waves and residual flow through the strait and their roles in the seasonal variation of the SCS circulation. The observations reveal that Qiongzhou Strait is an area where opposing tidal waves interact and a source of water transport to the Gulf of Beibu (Gulf of Tonkin), SCS. A year-round westward mean flow with a maximum speed of 10–40 cm s^{-1} is found in Qiongzhou Strait. This accounts for water transport of 0.2–0.4 Sv and 0.1–0.2 Sv into the Gulf of Beibu in winter–spring and summer–autumn, respectively. The outflow from Qiongzhou Strait may cause up to 44% of the gulf water to be refreshed each season, suggesting that it has a significant impact on the seasonal circulation in the Gulf of Beibu. This finding is in contrast to our current understanding that the seasonal circulation patterns in the South China Sea are primarily driven by seasonal winds. Several numerical experiments were conducted to examine the physical mechanisms responsible for the formation of the westward mean flow in Qiongzhou Strait. The model provides a reasonable simulation of semidiurnal and diurnal tidal waves in the strait and the predicted residual flow generally agrees with the observed mean flow. An analysis of the momentum equations indicates that the strong westward flow is driven mainly by tidal rectification over variable bottom topography. Both observations and modeling suggest that the coastal physical processes associated with tidal rectification and buoyancy input must be taken into account when the mass balance of the SCS circulation is investigated, especially for the regional circulation in the Gulf of Beibu.

1. Introduction

Qiongzhou Strait, located at 20°N, 109°–111°E, is a narrow ocean passage connecting the Gulf of Beibu (Gulf of Tonkin) on the west and the northeastern South China Sea (SCS) Basin on the east (Fig. 1). The strait is about 70 km long and 30 km wide, with a maximum depth of 120 m. This is a dynamic coastal region characterized by complex physical processes. Tidal waves, which are dominated by diurnal constituents on the western side and by semidiurnal constituents on the eastern side, propagate toward Qiongzhou Strait from the Gulf of Beibu and decrease significantly in amplitude

Corresponding author address: Changsheng Chen, School for Marine Sciences and Technology, University of Massachusetts–Dartmouth, 706 South Rodney French Blvd., New Bedford, MA 02744. E-mail: c1chen@umassd.edu

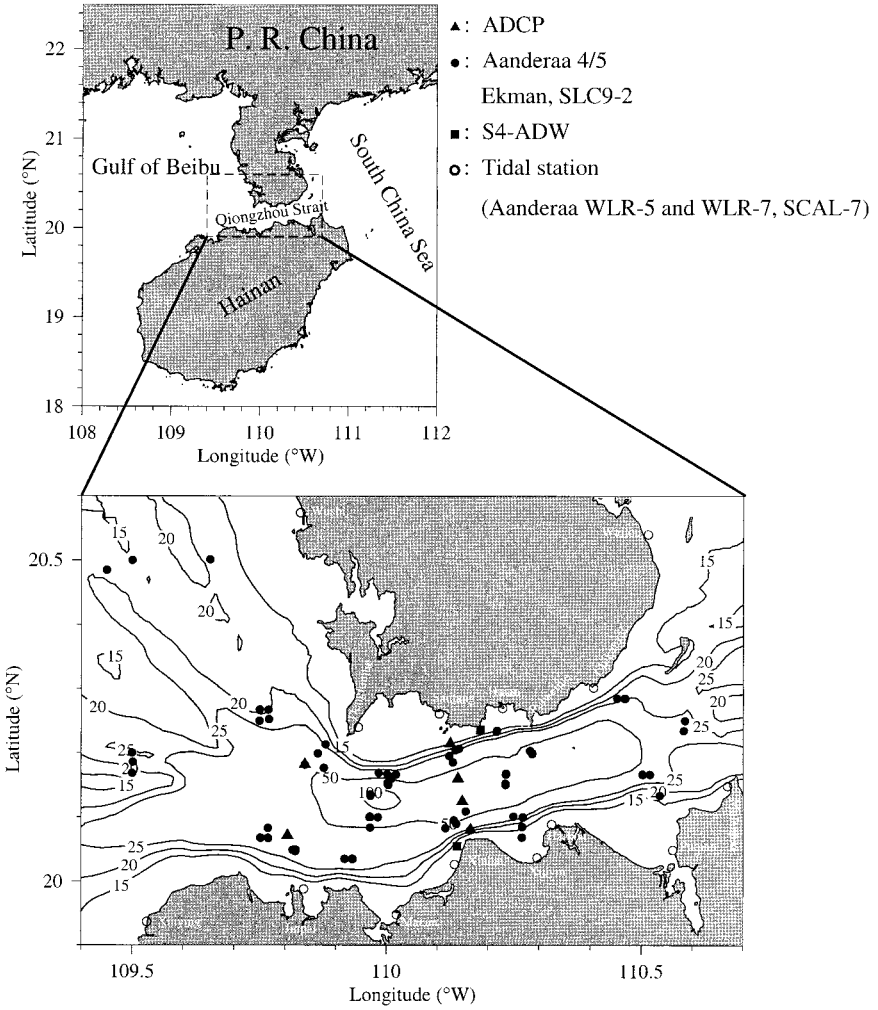

FIG. 1. Bathmetry of Qiongzhou Strait, South China Sea, and the sites of current and tidal measurements. The solid triangles, dots, and squares indicate types of current meters: ADCP, Aanderaa, Ekman, SLC9-2, and S4-ADW, respectively. The open circles are coastal tidal stations where Aanderaa WLR-5, Aanderaa WLR-7, and SCAL-7 pressure recorders were used to measure water level.

in the strait (Ding 1986; Cao and Fang 1990; Wang 1998). Strong tidal rectification over variable bottom topography and significant nonlinear interaction between diurnal and semidiurnal tides are expected in this strait. Both conditions could contribute directly to the formation of the residual current through the strait.

Our understanding of the current structure in Qiongzhou Strait is based primarily on the wind-induced seasonal circulation pattern in the SCS. According to the SCS circulation maps suggested by previous investigators (e.g., Yu and Liu 1993) (Fig. 2), during winter the SCS is characterized by a cyclonic circulation in the main basin, a southwestward current along the northern coast, and a cyclonic circulation in the Gulf of Beibu. As one of the water sources for the Gulf of Beibu, a westward flow is expected in Qiongzhou Strait. During summer, these circulation patterns are reversed, which leads to an eastward flow in Qiongzhou Strait. The seasonal pattern of the wind-induced large-scale SCS circulation has been described through observations (Wyrtki 1961; Shaw et al. 1996, 1999; Chu et al. 1997) and numerical simulations (Pohlmann 1987; Shaw and Chao 1994; Chao et al. 1996; Metzger and Hurlburt 1996; Chu et al. 1998; Liu et al. 2001). Recently, Liu et al. (2001) found that the circulation in the SCS is under a simple quasi-steady Sverdrup balance. The cyclonic and anticylconic circulations found in the SCS during winter and summer, respectively, are driven by the anomalous cyclonic and anticyclonic wind stress curls associated with seasonal patterns of the monsoon.

Little attention has been paid to the coastal region of the SCS, especially in Qiongzhou Strait. The seasonal current patterns in the strait shown in Fig. 2 are based mainly on a systematic guess following the large-scale

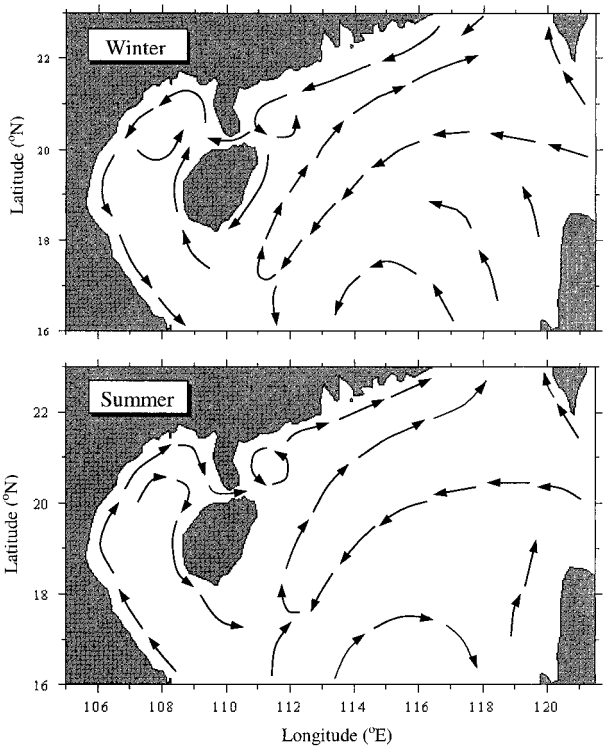

FIG. 2. Schematic of (top) wintertime and (bottom) summertime circulation patterns in the South China Sea suggested by wind-driven theory. This figure was plotted based on the seasonal patterns shown by Yu and Liu (1993).

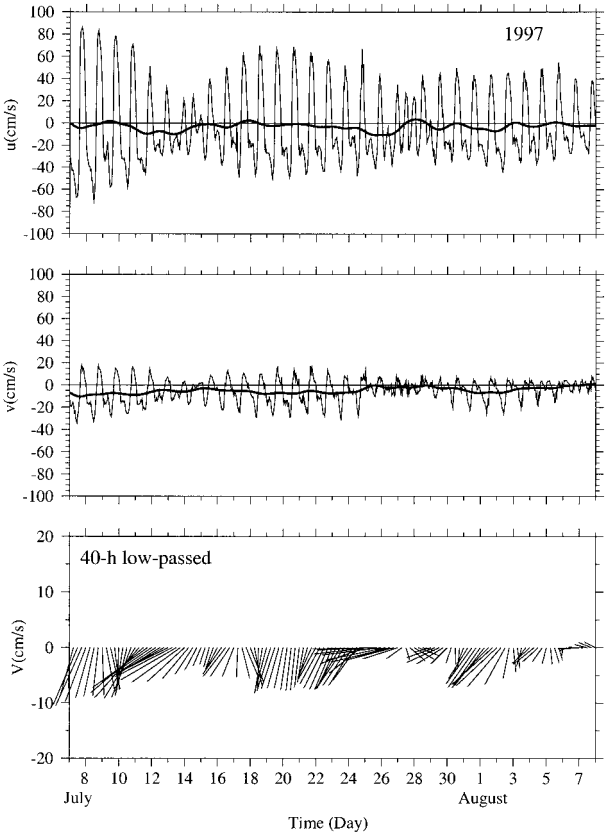

FIG. 3. Time series of the raw (u: upper and v: middle) and 40-h low-passed subtidal (lower) currents measured at the S4-ADW site in the northern Qiongzhou Strait. The heavy solid lines in the upper and middle panels are the x and y components of the 40-h low-pass subtidal currents.

wind-driven circulation. The complexity of tidal motions observed over the continental shelf of the northeastern SCS and Gulf of Baibu as well as in Qiongzhou Strait make us question whether or not the wind is a dominant force in the strait. Does the mean current in Qiongzhou Strait reverse seasonally? What is the role of Qiongzhou Strait in the seasonal variation of the coastal circulation and mass balance in the SCS? These questions have not been well explored.

Short- and long-term measurements of water level and currents have been made in Qiongzhou Strait since 1963. Water levels were recorded using pressure recorders at coastal tidal stations, and currents were measured using moored current meters. An analysis of these direct measurements is presented in this paper to describe the characteristics of the tidal motion and seasonal mean water circulation in Qiongzhou Strait.

A three-dimensional (3D) primitive equation model with turbulence closure was used to study the physical mechanisms responsible for the formation of the mean flow in Qiongzhou Strait. The model was forced by observed elevations and phases of M_2, O_1, and K_1 tides on both eastern and western open boundaries. A momentum balance analysis was conducted to examine the key physical processes that control the formation of the residual flow in the strait.

The remaining sections are organized as follows. In section 2, the measurement and data processing methods are described. In section 3, the distributions of tidal waves and currents are presented. In section 4, the seasonal patterns of the mean flow are estimated. In section 5, the model study is described and the effects of the strait on the seasonal variation of the circulation in the Gulf of Beibu and northeastern SCS Basin are discussed. Finally a summary is given in section 6.

2. The data

The sea surface elevation was recorded at tidal stations along the coast on both sides of Qiongzhou Strait using Aanderaa WLR-5, Aanderaa WLR-7, and SCAL-7 pressure recorders. Data were collected for over 30 years at the following stations: Xinying, Macun, Xinhai, Xiuyin, Santang, Haian, Sushi, and Wailou (Fig. 1). To resolve the detailed structure of tidal waves through the strait, four tidal gauges were set up temporally at Jinpai, Puqian, Paiweijue, and Dengloujue, and the sea surface elevation was measured every hour at these four stations over a month-long period in August of 1997 and 1998, respectively. The amplitudes and phases of six tidal con-

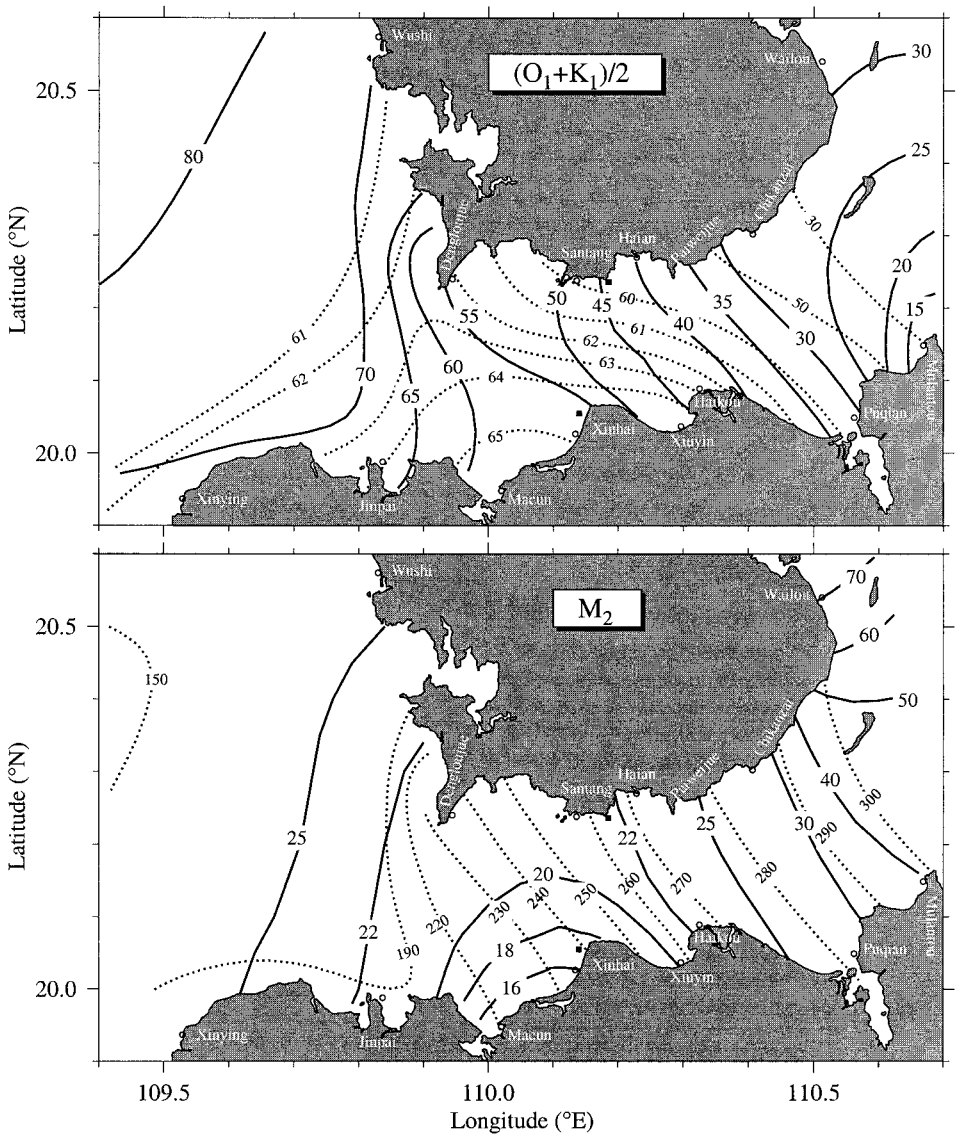

FIG. 4. Cotidal amplitudes (solid lines) and phases (dashed lines) of diurnal [$(O_1 + K_1)/2$] and semidiurnal M_2 tidal constituents. Units: coamplitude (cm) and cophase (deg).

stituents [three semidiurnal tides: M_2 (12.42 h), S_2 (12 h), N_2 (12.66 h); and three diurnal tides: O_1 (23.93 h), K_1 (25.82 h), and P_1 (24.07 h)] were estimated using a standard tidal harmonic analysis method. The surface tide in Qiongzhou Strait and adjacent coastal regions is dominated by the three major constituents M_2, O_1, and K_1, which account for about 80%–90% of the along-isobath current variation and kinetic energy in Qiongzhou Strait. Because of the similarity in amplitude and phase between O_1 and K_1, the diurnal tide is usually described by an average of O_1 and K_1 with an average period of 24.88 h, approximately twice the M_2 tidal period.

Five types of current meters [(ADCP), S4-ADW, Aanderaa, SLC9-2, Ekman] were deployed at mooring sites in Qiongzhou Strait and the Gulf of Beibu (Fig. 1). Instruments were deployed at standard levels of 0–3, 5, 10, 15, 30 m and near the bottom. Current data (speed and direction) were collected at these sites with a time interval of 15 min, 30 min, or 1 h over short-term (25 hours to 15 days) and long-term (month to year) periods at various times from 1963 to 1999.

Two approaches were used to filter tidal components from the current meter data. For data recorded over a period of one month or less, a least squares fit method was used to separate the tides from the raw data. Then an average was calculated over all residual records to construct a mean flow. In this case, only two major tidal constituents, M_2 and $(O_1 + K_1)/2$, were considered as the representatives of semidiurnal and diurnal tides, re-

TABLE 1. Comparison between observed and model-predicted amplitudes and phases of M_2 and $(K_1 + O_1)/2$ tidal constituents. (O: observed; M: model predicted.)

	M_2				$(K_1 + O_1)/2$			
	Amplitude (cm)		Phase (°)		Amplitude (cm)		Phase (°)	
Stations	O	M	O	M	O	M	O	M
Chikanzai	28.1	33.6	286.6	286.3	29.6	38.2	42.8	50.1
Dengloujue	21.0	11.5	234.0	251.2	54.6	50.3	62.3	59.0
Haian	22.1	23.9	267.0	279.2	41.0	43.3	55.7	53.0
Jinpai	21.3	20.9	199.5	201.3	68.7	60.2	64.1	66.5
Macun	15.6	20.8	226.0	223.2	57.2	57.4	65.7	66.5
Mulantou	40.1	42.8	298.4	281.0	14.8	36.7	29.2	62.8
Puqian	29.2	38.9	283.1	281.7	30.2	42.2	59.0	65.5
Santang	21.8	17.1	256.0	270.0	50.7	46.8	58.6	56.9
Wailuo	70.0	62.0	311.0	318.4	31.4	41.0	316.5	197.3
Wushi	28.5	25.2	160.0	160.1	72.9	64.3	59.4	65.1
Xinhai	15.7	21.1	251.6	239.2	57.7	53.7	64.9	65.3
Xinying	28.1	28.9	167.2	163.9	68.9	66.3	62.2	65.3
Xiuying	20.6	26.5	263.6	260.9	48.1	48.9	64.1	63.9

spectively, in the fitting. For data recorded over a period of longer than one month, the tidal currents were separated from the mean flow using an updated harmonic analysis method originally developed by Foreman (1979). This also was a least squares fit program with modification for nodal modulation and astronomical argument corrections. In this case, the low-frequency currents were calculated using a modified low-pass WH64 filter (a 129-point, symmetric weight filter with half-amplitude cutoff at 40 h, kindly provided by R. Beardsley at Woods Hole Oceanographic Institution). Examples of the raw and 40-h low-pass filtered current vectors taken in July–August 1997 are shown in Fig. 3.

3. Principal tidal elevation and current structures

It is well known that tidal waves propagate northward from the main SCS Basin and split into two major branches along the southern coast of Hainan Island (Wang 1998). When a tidal wave enters the Gulf of Beibu, the diurnal components of the wave grow significantly as a result of resonance with the local frequency of the gulf. Over the northeastern continental shelf of the SCS, the amplitude of the semidiurnal tides increases significantly toward the coast.

According to the distribution of co-phase lines, semidiurnal tides enter Qiongzhou Strait from the Gulf of Beibu, while the diurnal tides propagate through the strait mainly from the eastern side (Fig. 4 and Table 1). It is also evident that the diurnal tides propagate toward the strait from the Gulf of Beibu. The amplitude of the diurnal tide decreases eastward through the strait, with a value of 70 cm on the western end and 25 cm on the eastern end. The maximum phase is located near the southwestern coast of the strait, where tidal waves from both sides interact. The phase speed of the westward diurnal wave is about 10 m s^{-1}, which is much faster than the one that enters the strait from the western side. Unlike the diurnal tide, the amplitude of the semidiurnal M_2 tide increases eastward through the strait, with a value of 20 cm on the western entrance connecting the Gulf of Beibu and 40 cm on the eastern exit. The phase difference between the two ends of the strait is about 110 degrees (6.5 h), suggesting an average propagation speed of about 4.7 m s^{-1}, which is about 2 m s^{-1} slower than the diurnal tide. That both the diurnal and semidiurnal tides have significant alongstrait amplitude gradients implies an eastward divergence (for diurnal tides) or convergence (for semidiurnal tides) in Qiongzhou Strait.

The tidal ellipses for both diurnal and semidiurnal tides are oriented approximately parallel to the local topography, with their major axes along the strait (Figs. 5 and 6, Table 2). The diurnal tidal currents have their maximum amplitudes subsurface between 5 and 10 m, where the amplitude of the major axis varies in a range from about 30 cm s^{-1} in the western entrance connecting to the Gulf of Beibu to about 100 cm s^{-1} in the eastern region of the strait. Even at a depth close to the bottom (3 m above the bottom), the amplitude of the diurnal tidal currents reaches 30–50 cm s^{-1}.

The semidiurnal M_2 tidal current in Qiongzhou Strait ranges from 10 to 20 cm s^{-1}, one order of magnitude smaller than the maximum diurnal tidal current. Unlike the diurnal tidal currents, the amplitude of the M_2 tidal current exhibits relative uniformity in the vertical, such that the tidal current near the bottom is comparable to that found near the surface.

To a certain extent, our findings in this study disagree with previous tidal analysis results in the SCS (Cao and Fang 1990; Wang 1998). Our analysis shows that the M_2 tidal wave propagates eastward through Qiongzhou Strait, and the diurnal tidal waves enter the strait from both western and eastern entrances. These results are completely different from our previous understanding that the M_2 and diurnal tidal waves propagate westward and eastward through the strait, respectively. In fact, most of the previous tidal analysis results were based

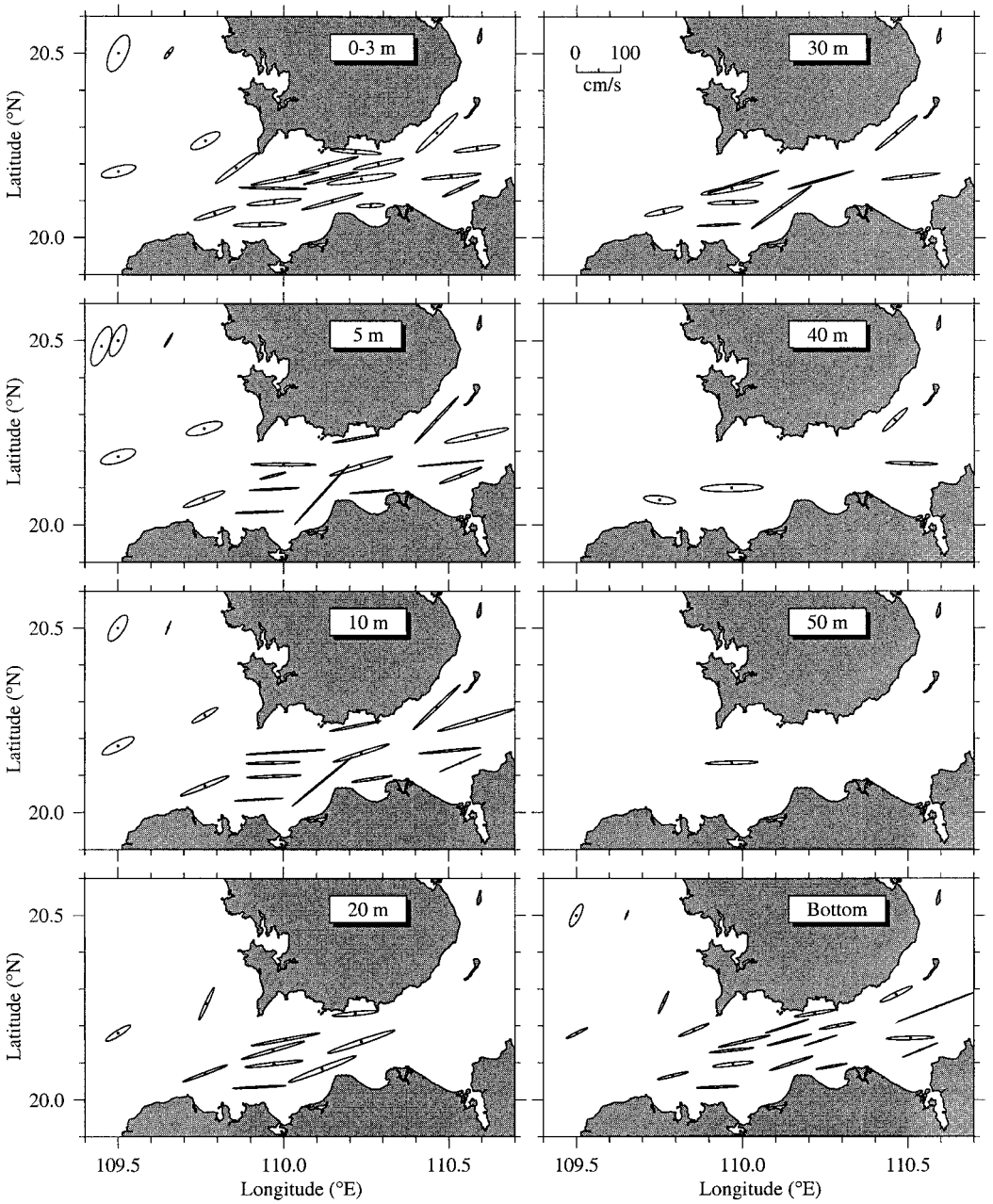

FIG. 5. Tidal ellipses of the diurnal tidal current [an average of $(O_1 + K_1)/2$] at selected depths of 0–3, 5, 10, 20, 30, 40, and 50 m and near the bottom (3 m above the bottom).

on either numerical tidal simulations or a few nearly coastal tidal records. Until this study, no detailed tidal analysis had been conducted using long-term surface elevation records from both sides of Qiongzhou Strait and the adjacent coastal region.

Alongstrait and vertical distributions of tidal currents are consistent with the alongstrait distribution of tidal elevation. The large amplitude and remarkable variation of tidal currents observed in such a shallow strait imply that strong nonlinear interaction might be active in this region, and thus a relatively strong tidal residual flow should be expected along the strait. A detailed discussion of the residual flow is given next.

4. The mean flow field

The mean flow is determined by the seasonal average of residual currents at each measurement site. A season is defined based on tropical climatic conditions in which winter is December–February, spring is March–May, summer is June–August, and autumn is September–November. The seasonal variation of air temperature in

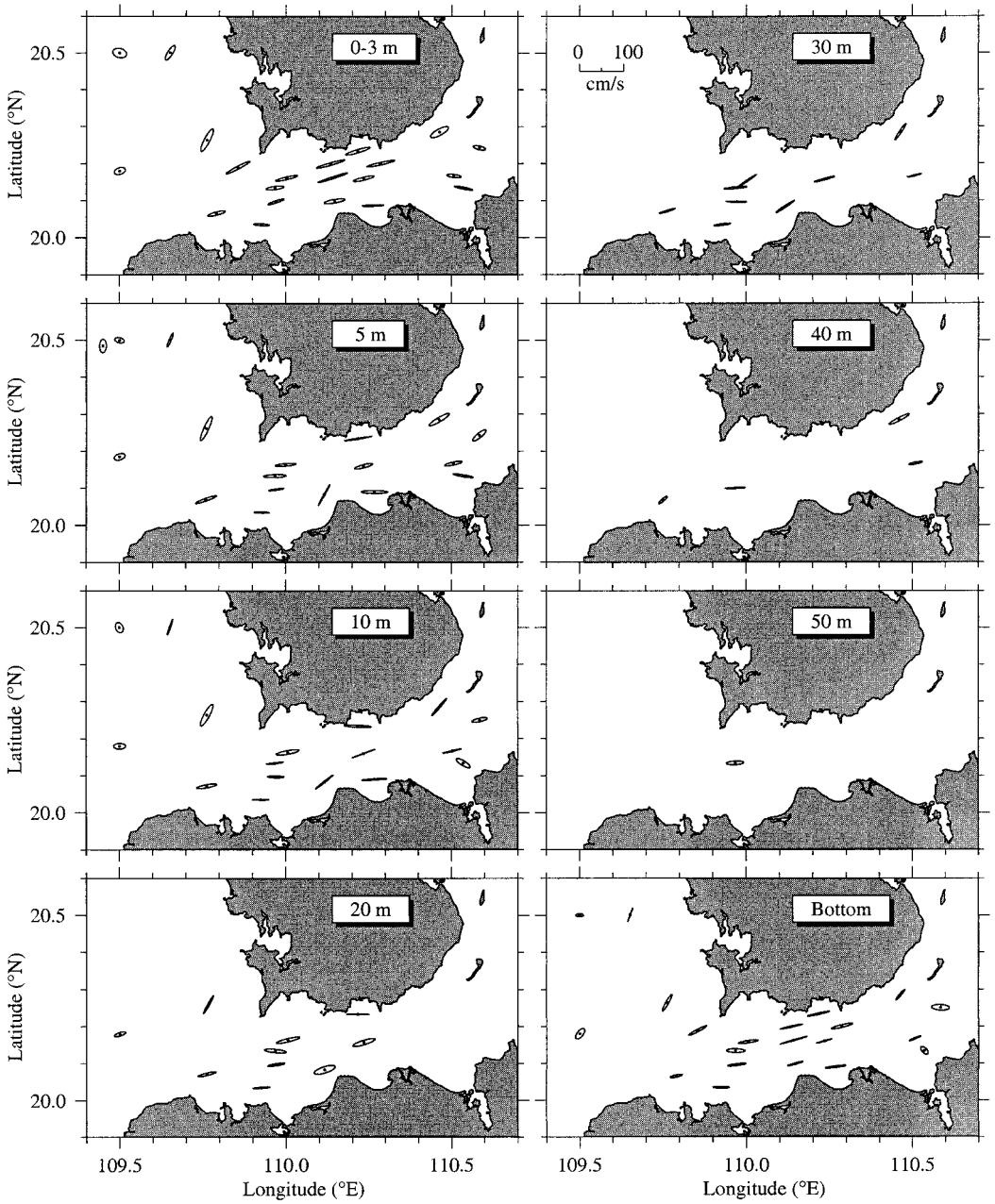

FIG. 6. Tidal ellipses of the semidiurnal M_2 tidal current at selected depths of 0–3, 5, 10, 20, 30, 40, and 50 m and near the bottom (3 m above the bottom).

Qiongzhou Strait is relatively small, with a maximum difference of 7°C between summer and winter and an annual average air temperature of about 23.8°C. The wind field, however, exhibits a significant seasonal variation, dominated by northeasterly winds in winter and spring and by southeasterly winds in summer and autumn. The average wind speed is about 2.7 m s^{-1} in winter and spring and about 2.8 m s^{-1} in summer and autumn, but the maximum wind speed exceeds 10 m s^{-1} in winter and 24 m s^{-1} in summer as atmospheric fronts and storms pass (Wang 1998).

The synthetic analysis of all current data available over the last 37 years shows that there is a year-round westward mean flow in Qiongzhou Strait (Figs. 7–10). The current is stronger in the upper 10 m, relatively weak at middepth, and significant near the bottom, with a maximum speed of about 20–40 cm s^{-1} in winter and spring and of 10–30 cm s^{-1} in summer and autumn. In

TABLE 2. Parameters of tidal ellipses.

Number	Lat (°N)	Long (°E)	Depth (m)	M_2				$(K_1 + O_1)/2$			
				$\hat{U}_{max}$ (m)	$\hat{U}_{min}$ (m)	θ_{orient} (deg-G)	θ_{phase} (deg-G)	$\hat{U}_{max}$ (m)	$\hat{U}_{min}$ (m)	θ_{orient} (deg-G)	θ_{phase} (deg-G)
1	20.50	109.50	3	15.79	9.38	−11.01	81.65	40.88	18.64	61.12	59.57
			5	11.77	6.04	21.44	115.01	37.95	14.16	63.59	21.58
			10	11.04	8.03	−60.49	129.56	32.12	13.07	51.40	109.88
			Bottom	8.82	2.88	1.49	128.37	26.11	8.51	58.85	71.77
2	20.18	109.50	3	12.93	6.78	14.31	28.31	39.93	10.46	12.33	110.26
			5	12.76	6.16	15.08	14.42	41.02	12.22	15.25	83.57
			10	13.40	5.75	0.60	14.94	39.51	9.85	24.44	80.55
			20	12.99	3.70	16.39	6.74	31.96	6.04	28.87	107.07
			Bottom	13.60	6.45	45.69	42.67	26.42	2.56	24.10	108.81
3	20.50	109.65	3	17.76	5.48	54.64	119.33	15.13	3.72	49.09	25.96
			5	15.67	2.33	64.13	120.17	16.68	1.73	55.90	43.48
			10	16.70	1.41	68.88	132.18	14.74	0.63	65.29	44.69
			Bottom	15.05	0.56	66.63	129.04	10.26	0.75	64.83	43.16
4	20.26	109.76	3	26.21	6.22	59.81	77.70	36.18	10.77	25.20	61.49
			5	27.18	5.27	63.19	44.87	41.84	10.63	14.12	81.17
			10	25.75	5.96	57.69	43.52	32.74	5.34	27.67	65.60
			20	21.15	1.97	58.26	66.21	36.94	3.62	62.69	103.89
			Bottom	19.46	3.11	57.72	68.53	25.13	2.67	62.90	81.88
5	20.07	109.79	3	20.03	3.27	12.67	53.56	48.66	4.67	16.28	58.54
			5	24.58	2.71	17.74	87.74	49.30	5.86	18.97	61.02
			10	22.63	3.20	9.38	44.34	57.92	4.66	20.04	55.96
			20	20.47	2.51	12.41	50.88	52.75	2.69	18.62	83.99
			30	18.41	1.49	15.82	28.19	44.05	5.11	11.39	85.48
			40	11.76	2.58	37.96	39.01	36.38	7.89	−5.86	133.52
			50	19.58	3.71	2.49	82.67	58.93	3.50	1.21	26.50
			Bottom	13.44	2.33	10.63	37.45	35.01	2.68	12.05	68.71
6	20.19	109.86	3	29.59	2.87	25.28	86.42	56.85	5.45	33.57	110.40
			Bottom	22.15	2.46	25.29	95.36	36.16	3.09	20.59	90.68
7	20.04	109.93	3	17.34	2.03	−3.27	77.84	59.54	4.25	1.32	81.17
			5	16.78	1.24	−1.24	40.33	53.86	1.62	1.98	93.20
			10	19.20	0.72	−0.41	39.95	53.82	1.15	2.95	99.58
			20	18.90	1.11	3.61	54.22	59.60	1.54	2.66	103.72
			30	18.84	1.64	5.95	22.78	47.39	1.92	2.68	92.66
			Bottom	18.25	1.78	−0.23	44.13	47.09	1.88	1.88	103.45
8	20.16	110.00	3	24.86	2.68	11.89	50.61	77.67	3.50	9.87	55.98
			5	23.29	2.57	4.20	77.89	73.56	2.77	−0.21	62.10
			10	25.76	3.79	9.22	117.26	87.86	1.44	3.04	80.80
			20	26.59	3.43	12.16	97.58	78.32	2.64	9.37	80.17
			30	24.75	1.38	31.23	134.50	82.71	2.05	16.20	91.20
			Bottom	22.39	2.40	7.60	52.96	58.61	2.55	11.68	60.00
9	20.13	109.97	3	19.92	3.29	6.22	100.26	75.38	2.14	−0.97	67.72
			5	24.61	3.14	1.93	19.38	29.58	2.09	13.29	50.68
			10	17.78	0.95	6.01	45.69	59.60	2.51	1.48	45.85
			20	24.28	3.45	−5.33	106.12	73.19	3.24	14.41	48.98
			30	25.76	1.86	4.56	105.81	70.42	5.84	9.53	47.11
			Bottom	20.27	3.95	−1.22	97.27	49.15	2.19	5.57	31.90
10	20.10	109.97	3	18.50	2.24	16.64	65.99	61.11	4.75	5.42	78.91
			5	16.35	1.33	6.26	65.72	55.09	1.60	2.52	48.44
			10	18.15	1.91	−1.05	58.16	61.19	2.59	2.20	55.01
			20	19.09	2.12	7.91	54.93	64.64	3.30	5.63	57.33
			30	21.78	1.00	−0.66	63.09	56.60	4.05	1.91	69.72
			40	22.52	0.96	2.04	27.38	70.27	7.66	0.97	113.17
			Bottom	20.20	1.94	6.22	65.57	45.54	3.76	5.65	66.48

winter and spring, the near-bottom mean flow in the strait reaches 10–15 cm s^{-1}, which is comparable to that found near the surface. The same tendency is also found in summer, even though the speed of the mean flow throughout the whole water column is relatively weaker.

The mean transport of the outflow from Qiongzhou Strait to the Gulf of Beibu is estimated on a cross-strait transect with an average width of 29.5 km and an average depth of 46 m. Considering the current speed of 20–40 cm s^{-1} at the surface and 10–15 cm s^{-1} at the bottom in winter through spring and 10–30 cm s^{-1} at the surface and 5–10 cm s^{-1} at the bottom in summer through autumn, the mean transport of the outflow is 0.2–0.4 Sv (Sv $\equiv 10^6$ m^3 s^{-1}) in winter through spring and 0.1–0.2 Sv in summer through autumn.

TABLE 2. (*Continued*)

Number	Lat (°N)	Long (°E)	Depth (m)	M_2				$(K_1 + O_1)/2$			
				$\hat{U}_{max}$ (m)	$\hat{U}_{min}$ (m)	θ_{orient} (deg-G)	θ_{phase} (deg-G)	$\hat{U}_{max}$ (m)	$\hat{U}_{min}$ (m)	θ_{orient} (deg-G)	θ_{phase} (deg-G)
11	20.20	110.13	3	33.13	2.57	14.15	48.88	68.58	3.25	13.20	63.45
			Bottom	24.75	1.19	11.07	39.65	50.05	1.49	16.17	41.86
12	20.16	110.14	3	34.39	1.91	16.16	39.78	63.31	2.71	11.66	66.90
			Bottom	30.13	0.80	14.29	54.40	51.27	1.83	13.10	65.99
13	20.10	110.15	3	23.65	3.63	8.62	49.98	71.04	3.23	13.93	64.90
			5	24.43	0.93	58.34	44.83	85.91	1.26	44.56	119.41
			10	23.77	1.21	35.56	34.91	82.25	1.35	36.42	124.44
			20	24.14	6.39	15.45	39.29	80.72	5.12	19.07	124.22
			30	23.66	1.79	30.57	39.33	80.11	2.78	32.94	123.72
			Bottom	17.70	1.30	14.11	55.31	50.15	2.56	16.47	64.31
14	20.23	110.22	3	28.16	3.32	14.74	52.59	57.56	4.11	−3.93	125.13
			5	30.56	1.00	8.18	65.53	52.25	2.18	9.02	123.51
			10	29.56	2.27	−2.28	42.05	57.89	2.36	10.28	114.02
			20	25.52	0.37	−0.32	67.53	51.62	4.08	4.85	112.45
			Bottom	25.38	1.49	11.25	45.74	46.43	3.12	8.60	111.29
15	20.16	110.23	3	23.97	3.11	12.22	66.53	78.54	6.38	7.16	86.45
			5	20.72	3.24	13.02	54.09	73.95	4.16	15.22	65.44
			10	27.55	0.31	18.60	23.64	65.53	3.56	16.19	64.73
			20	25.54	4.48	14.94	63.38	79.26	4.94	16.76	45.96
			30	23.57	1.65	13.82	62.82	74.95	1.88	14.24	47.38
			Bottom	17.67	0.59	14.39	78.57	37.87	0.80	15.87	65.21
16	20.09	110.26	3	24.30	1.54	1.88	56.27	31.72	4.03	2.43	76.36
			5	29.62	3.00	−0.35	45.73	49.57	1.55	4.02	44.53
			10	27.05	1.17	2.92	45.46	45.83	2.52	7.84	44.91
			20	25.10	3.38	3.88	6.19	49.62	1.46	−1.93	90.09
			Bottom	23.00	1.47	6.35	49.24	35.30	1.90	9.34	43.17
17	20.20	110.29	3	32.06	2.58	11.46	101.21	58.13	4.22	10.90	92.61
			Bottom	24.09	2.75	12.38	78.01	39.91	2.86	9.83	90.98
18	20.29	110.46	3	22.46	6.52	25.46	58.68	61.68	6.30	40.35	74.53
			5	25.46	4.52	27.71	83.61	68.13	2.53	43.84	81.84
			10	24.04	2.02	45.80	56.25	69.70	3.00	40.68	71.93
			20	20.97	1.78	18.84	79.91	64.91	3.80	40.21	70.97
			30	20.62	2.49	52.85	58.56	58.73	3.79	36.86	70.40
			40	24.81	3.26	24.58	48.65	36.82	5.27	40.26	95.37
			Bottom	13.93	2.03	46.68	37.85	39.63	4.72	23.39	74.15
19	20.17	110.51	3	16.25	3.12	−5.78	87.12	66.79	3.58	4.71	56.16
			5	20.17	2.98	10.28	90.20	73.74	1.04	4.52	50.58
			10	20.58	0.96	12.09	120.45	70.08	2.05	4.82	18.51
			20	19.10	0.73	10.70	91.33	71.81	2.32	5.09	54.04
			30	15.83	1.10	12.61	49.56	65.92	3.21	5.52	54.59
			40	15.42	2.00	9.72	61.85	58.82	3.10	−1.48	80.47
			Bottom	13.60	1.27	19.79	75.19	53.37	3.68	1.43	52.63
20	20.13	110.54	3	20.99	2.02	−10.35	90.85	44.43	2.87	22.41	129.96
			5	22.51	1.95	−8.51	91.16	50.28	3.38	18.79	128.61
			10	17.62	5.03	−27.93	98.41	48.99	0.24	21.03	128.36
			Bottom	9.91	5.34	−40.37	120.28	41.28	0.68	19.95	124.30
21	20.24	110.58	3	14.28	3.81	−12.11	29.34	52.29	4.43	6.97	24.04
			5	18.07	4.85	35.73	22.17	73.95	5.84	11.07	3.66
			10	17.25	3.69	10.62	36.32	91.56	3.73	14.61	4.35
			Bottom	20.20	5.77	−2.56	29.65	91.88	0.63	18.99	2.70

The wintertime current pattern observed in Qiongzhou Strait is the same as that suggested by previous investigators based on the wind-induced circulation in the SCS. The wind-induced theory, however, fails to predict the summertime current pattern observed in the strait. The observations in the last 37 years show a significant westward flow through Qiongzhou Strait, in direct contrast to the eastward flow predicted by wind-driven theory.

5. A model-guided mechanism study

The fact that the mean flow direction observed in summer through autumn in Qiongzhou Strait opposes that suggested by previous investigators implies that the subtidal current is driven by physical processes other than large-scale wind forcing. What causes the formation of the permanent westward flow in Qiongzhou Strait—buoyancy forcing or tidal rectification? Recent-

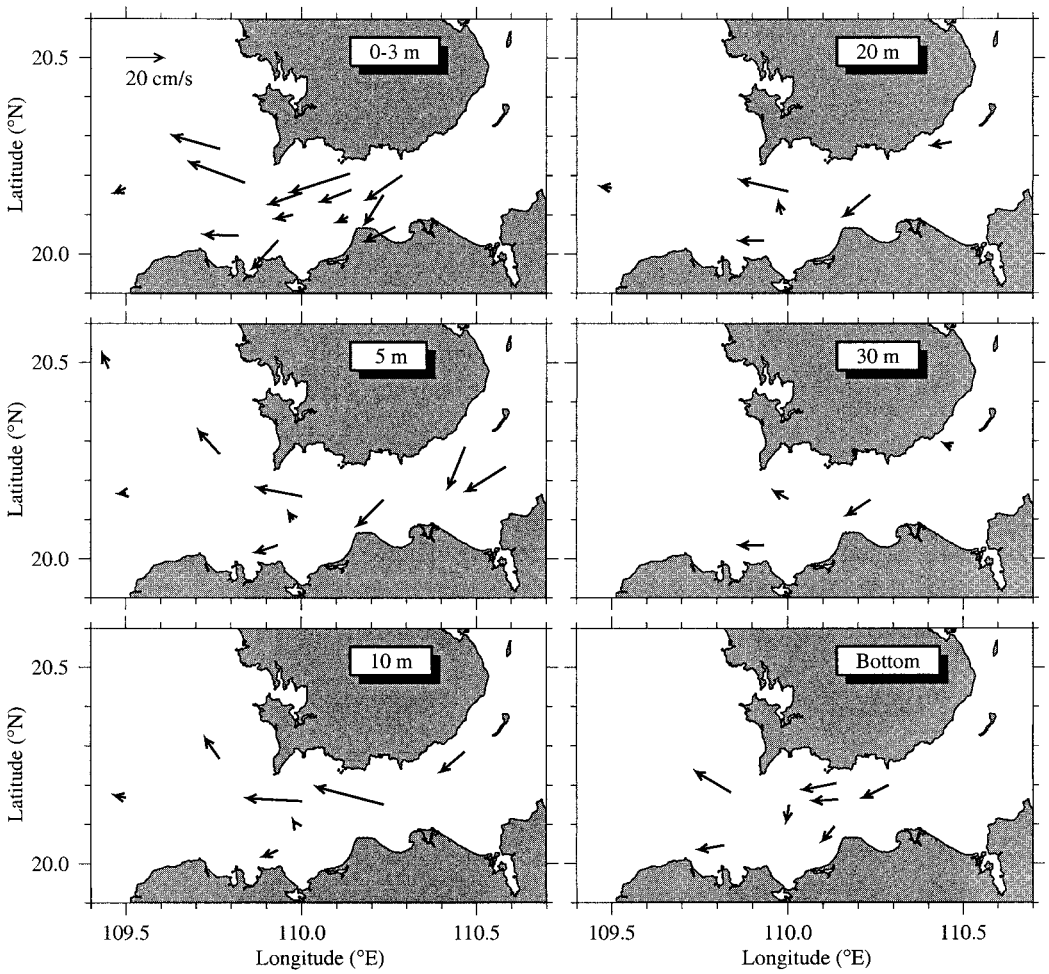

FIG. 7. Vectors of the wintertime mean flow at selected depths of 0–3, 5, 10, 20, and 30 m and near the bottom. The vector scale is indicated in the upper right panel.

ly, there is evidence of southward intrusion of relatively cold and less saline water along the northeastern coast of the SCS in spring and summer (Huang 1994). This water, which originally came from rivers along the coast of Guangdong Province, flows southwestward and then southward along the Leizhou Peninsula and enters Qiongzhou Strait from the east. We carefully examined the historical hydrographic survey data taken in the SCS and found a significant annual variability of the buoyancy flow over the northeastern shelf. For example, in June 1981, the river discharge–induced, relatively low salinity water flowed southwestward along the coast and entered Qiongzhou Strait. However, in August 1982, this water was trapped upstream in the northeast, near the river mouth, due to the southwesterly monsoon (Fig. 11). Since westward mean flow has been the norm in Qiongzhou Strait over the past 37 years and because low-salinity water is not always evident over the coastal region at 20°N in summer, we conclude here that this buoyancy-driven coastal flow is not an essential physical process generating the observed westward mean current in Qiongzhou Strait.

The eastward decrease in the amplitude of the diurnal tide indicates a significant divergence of tidal-induced water flux. This type of divergence tends to increase in the eastward direction. Similarly, the semidiurnal M_2 tidal flux increased westward, resulting in a divergence in the westward direction. These observations suggest that strong tidal rectification occurs in the strait due to the convergence and divergence of the momentum flux of tidal currents. Seasonal variation of the mean flow in Qiongzhou Strait indirectly supports the existence of a year-round westward tidally rectified flow. Since tide- and wind-induced mean flows are in the same direction in winter through spring and oppose each other in summer through autumn, the westward mean flow in Qiongzhou Strait is stronger in winter than summer.

According to the theory of tidal rectification over variable topography where bottom friction is dominant, the tidally rectified residual current usually flows along

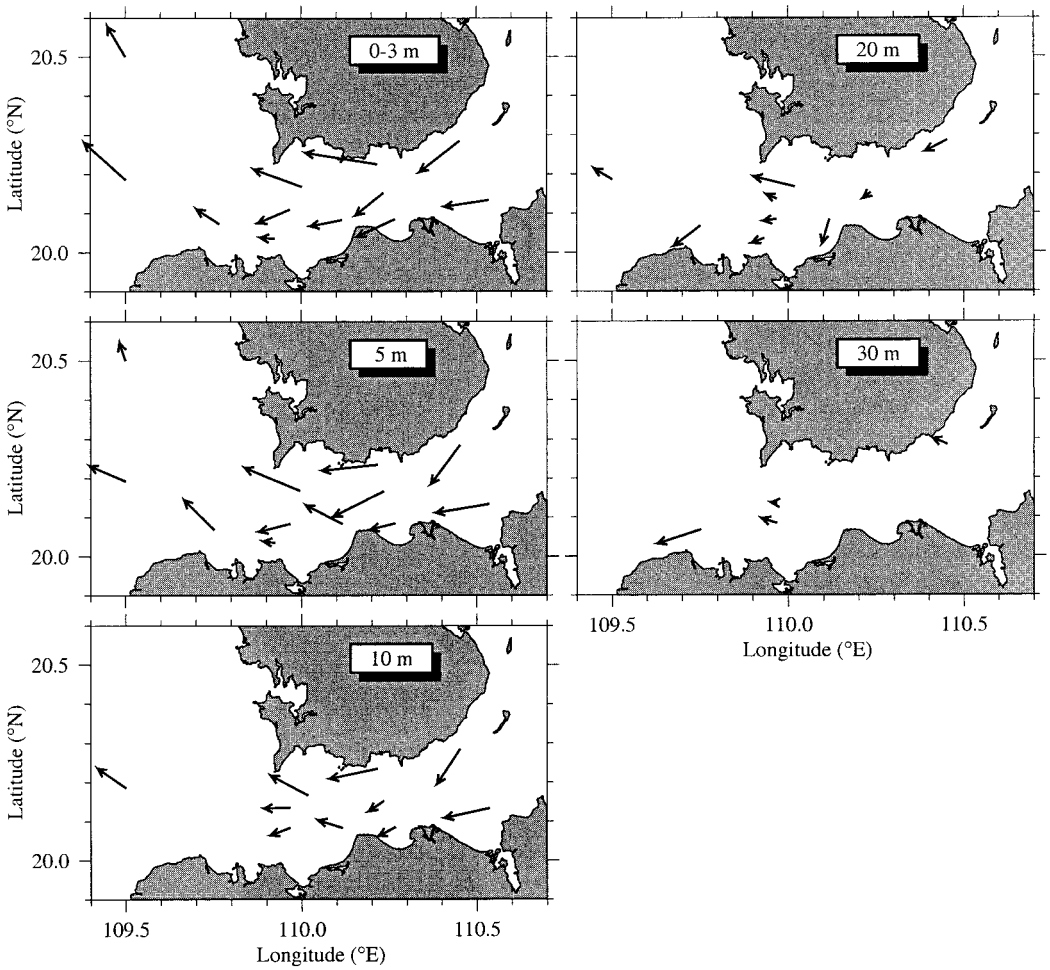

FIG. 8. The vectors of the springtime mean flow at selected depths of 0–3, 5, 10, 20, and 30 m. The vector scale is the same as that shown in Fig. 7.

the local isobath, with the shallow slope on its right (Loder 1980; Chen and Beardsley 1995). If this theory is applied to Qiongzhou Strait, the residual current should flow eastward along the southern coast and westward on the northern coast, forming an eddylike cyclonic mean circulation along the closed isobaths in the center of the strait. However, we found no such significant eddylike circulation pattern in the strait.

Chen et al. (1999) studied the tidal rectification process along the inner shelf of the South Atlantic Bight. They found that, when tidal nonlinear advection and cross-isobath surface pressure gradient are dominant, the tidally rectified current could flow along the local isobath with the shallow coast on its left, a direction which is opposite to the tidally rectified flow controlled by combined tidal advection and bottom friction found by Loder (1980) and Chen and Beardsley (1995). Provided that the ideas presented in Chen et al. (1999) apply to Qiongzhou Strait, the mean sea level should increase northward across the strait, or the alongstrait gradient of the mean sea level should be one order of magnitude smaller than the nonlinear tidal advection. A large tidal advection is expected in Qiongzhou Strait since tidal currents are very strong and the cross-strait slope of bottom topography is large. During summer, the observed mean sea level is generally about 1 cm higher at Santang (on the northern coast) than at Xinghai (on the southern coast), even during a period when the southwesterly monsoon wind prevails. This cross-isobath sea level gradient could generate a westward flow of 10–15 cm s^{-1} in the strait, which accounts for about 50%–60% magnitude of the westward mean flow observed in the strait. All these factors suggest that the tidal rectification mechanism proposed by Chen et al. (1999) might be responsible for the formation of the westward mean flow in Qiongzhou Strait.

To verify this tidal rectification mechanism, we have used a 3D primitive equation numerical model with turbulence closure as a tool for examining the physical processes in Qiongzhou Strait. This model (called

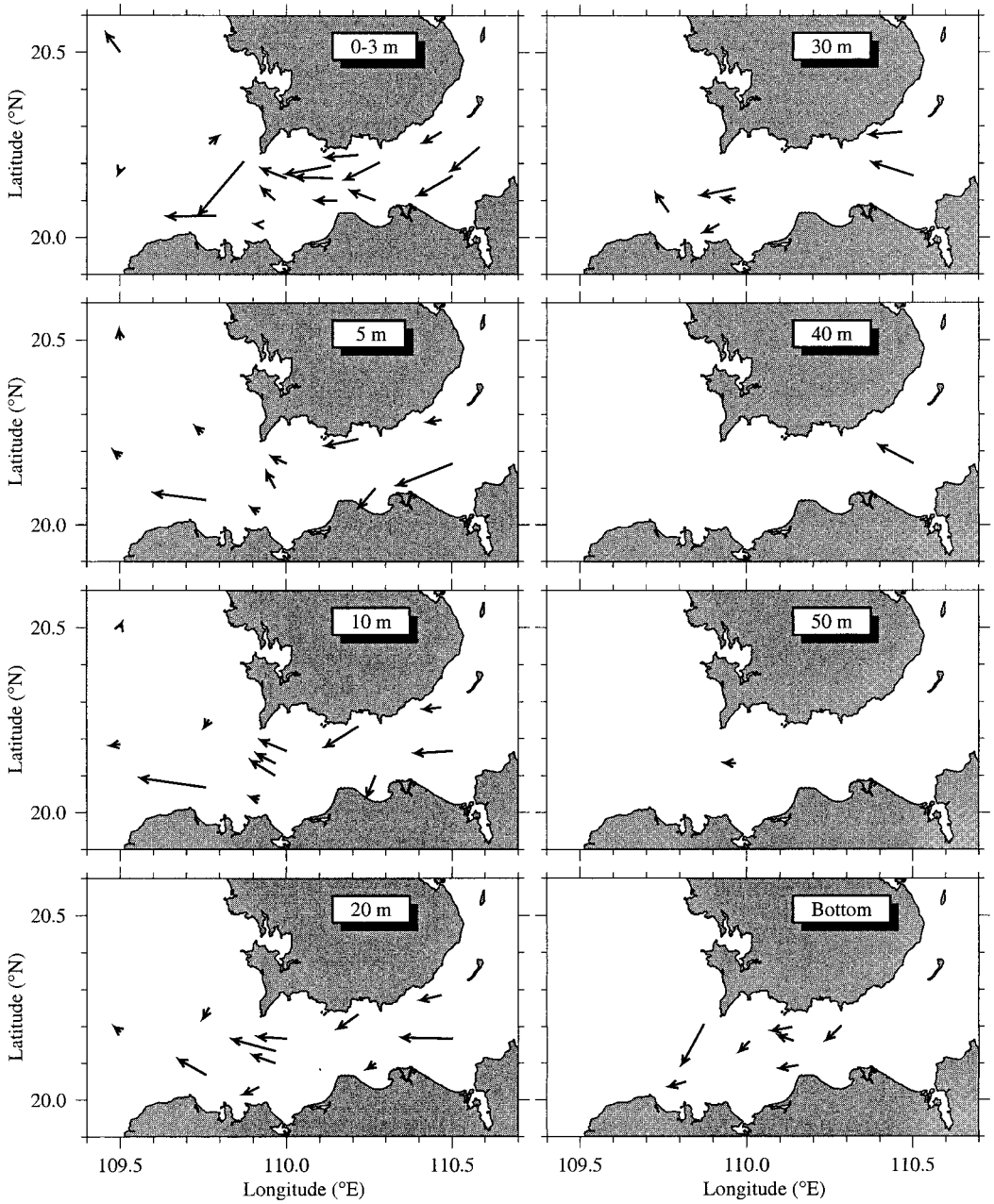

FIG. 9. The vectors of the summertime mean flow at selected depths of 0–3, 5, 10, 20, 30, 40, and 50 m and near the bottom. The vector scale is the same as that shown in Fig. 7.

Ecom-si) was developed originally by Blumberg and Mellor (1987) and modified by Chen and Beardsley (1995, 1998) and Chen et al. (1999). The model uses the σ coordinate in the vertical and curvilinear orthogonal coordinates in the horizontal. The model incorporates the semi-implicit scheme developed by Casulli (1990) that allows the barotropic pressure gradient in the momentum equations and the velocity convergence in the continuity equation to be treated implicitly. A detailed description of an updated version of the model was given in Chen et al. (2001).

The numerical model domain covered the entire area of Qiongzhou Strait with open boundaries running from Yangpu to Beihai on the western side and from Baihu to Dianbai on the eastern side (Fig. 12). A uniform horizontal grid with a horizontal resolution of 1.7 km was used. Sixteen uniform σ levels were specified in the vertical. This provided a vertical resolution of 1–5

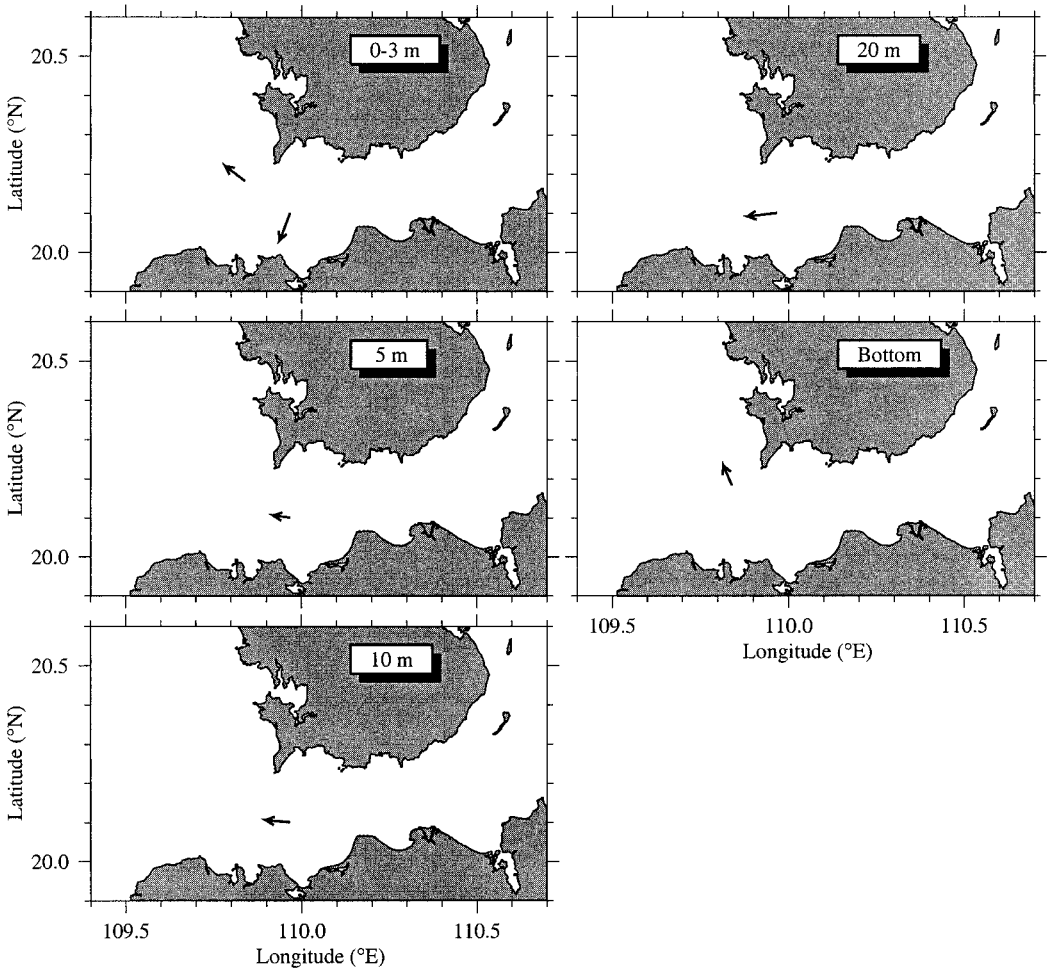

FIG. 10. The vectors of the autumn time mean flow at selected depths of 0–3, 5, 10, and 20 m and near the bottom. The vector scale is the same as that shown in Fig. 7.

m over the depth range 15–75 m near the coast and the western or eastern areas off the strait, and 8 m in the central area of the strait where water depth is 120 m. The bottom depth at each model grid point was interpolated from a Chinese bathymetric map. The model time step was 298.52 sec, resulting in 300 time steps over an average period of O_1 and K_1.

The model was forced on the western and eastern open boundaries by the M_2, O_1, and K_1 tidal forcings. The surface elevations and phases specified on open boundaries were interpolated directly from tidal amplitudes and phases observed at the southern and northern coastal tidal stations of Yangpu and Beihai (on the west) and Baohu and Dianbai (on the east). A radiation condition for currents was applied at each of the open boundaries to minimize energy reflection into the computational domain (Chen et al. 1995). To focus on the tidal rectification process, the temperature and salinity were specified as constant values of 25°C and 35 Psu. The model was run as an initial value problem with tidal forcing for one month. The M_2, O_1, and K_1 constituents were separated from the model-predicted surface elevation and current data using a least squares fitting method, and model-predicted residual currents were defined as the average currents after tides were removed.

The model provides a reasonable simulation of the tides in Qiongzhou Strait. The model-predicted M_2 tide enters the strait from the Gulf of Beibu, while the diurnal tide propagates into the strait from the eastern side (Fig. 13). The amplitude of the diurnal tide increases westward through the strait, with a value of 35 cm on the eastern end and 60 cm on the western end. The maximum phase is located near the southwestern coast of the strait, where tidal waves from both sides interact. The amplitude of the semidiurnal M_2 tide increases eastward through the strait, with a value of 20 cm at the eastern entrance connecting the Gulf of Beibu and 45 cm at the eastern exit. The phase difference between the two ends of the strait is about 110 degrees. The model-predicted amplitudes and phases of M_2 and $(O_1 + K_1)/2$

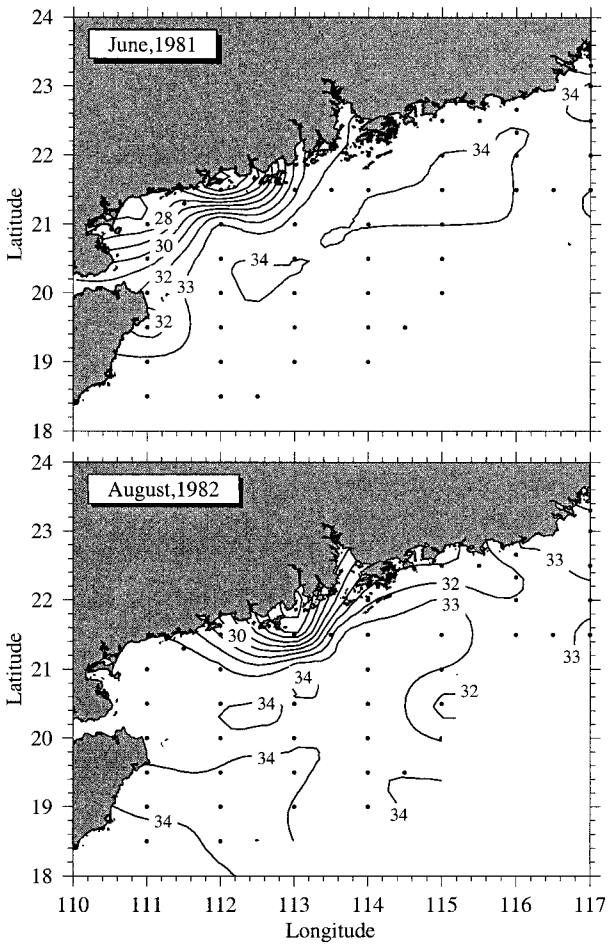

FIG. 11. Distribution of the surface salinity over the northeastern shelf of the SCS in Jun 1981 and Aug 1982. The measurement stations are indicated by dots.

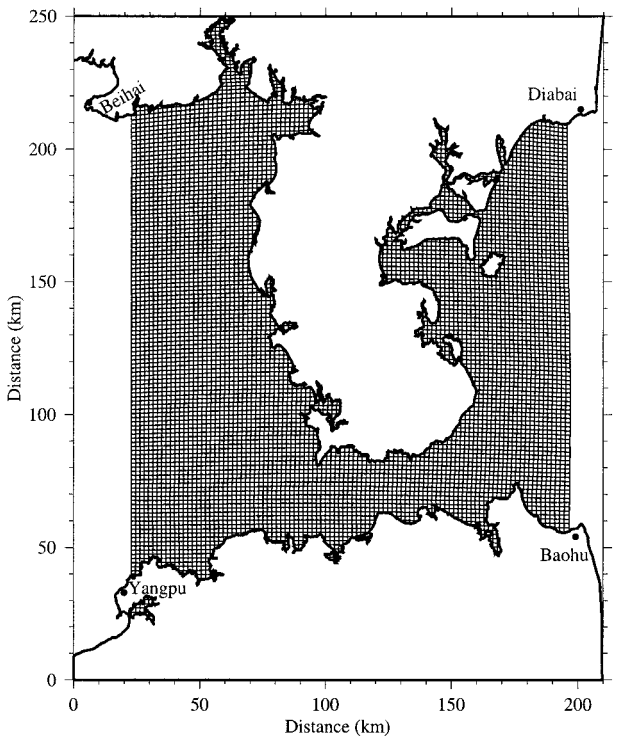

FIG. 12. Numerical grids for Qiongzhou Strait tidal model. The computational domain covers the entire area of Qiongzhou Strait with open boundaries running from Yangpu to Beihai on the western side and from Baihu to Dianbai on the eastern side.

tides were in reasonable agreement with observed data taken at coastal tidal stations except those at Wailou, Wushi, Puqian, and Mulantou (Table 1). The large disparity between model-predicted and observed amplitudes and phases at these stations is probably caused by the relatively poor resolution of bottom topography around those areas. For example, there is a trough area on the slope around Puqian, which is not resolved in our model. The model predicts a node point of the M_2 tide around Dengloujue. This node point was reported in the historical data, but does not appear in the recent tidal measurements. This suggests that the tidal structure around that area has changed, so a more accurate tidal simulation must be conducted using the updated geometric data. On the other hand, since these model/observation differences would not change the ''synoptic'' nature of the residual flow in the strait, they are acceptable if the modeling study is focused on the physical mechanism responsible for the formation of the westward flow in Qiongzhou Strait.

The model predicts a relatively strong westward tidally rectified current in Qiongzhou Strait (Fig. 14). This current is generally stronger on the northern coast, with several cyclonic or anticyclonic eddies in the southern region inside and outside the strait. The maximum current is about 40 cm s^{-1}. Relatively strong eddylike currents found near the eastern end of the strait are clearly driven by the complex bottom topographic slope there since they disappear when the bottom topography is smoothed. Whether these eddylike currents exist or not around the eastern boundary, they show no significant influence on the magnitude and pattern of the westward residual flow inside the strait. This suggests that the westward current is driven locally by tidal forcing rather than by the ''remote'' input from these eddylike currents.

The direction, magnitude, and cross-isobath distribution of the model-predicted residual flow is in good agreement with the mean currents observed in Qiongzhou Strait over the past 37 years. This clearly demonstrates that this current is driven by the interaction of tidal currents over the strait's variable bottom topography. To examine the contribution of each tidal constituent to the residual flow, we also did numerical experiments by forcing the model with individual M_2, O_1, and K_1 tides. The model results show that the residual flow in the strait is dominated by diurnal (O_1 and K_1)

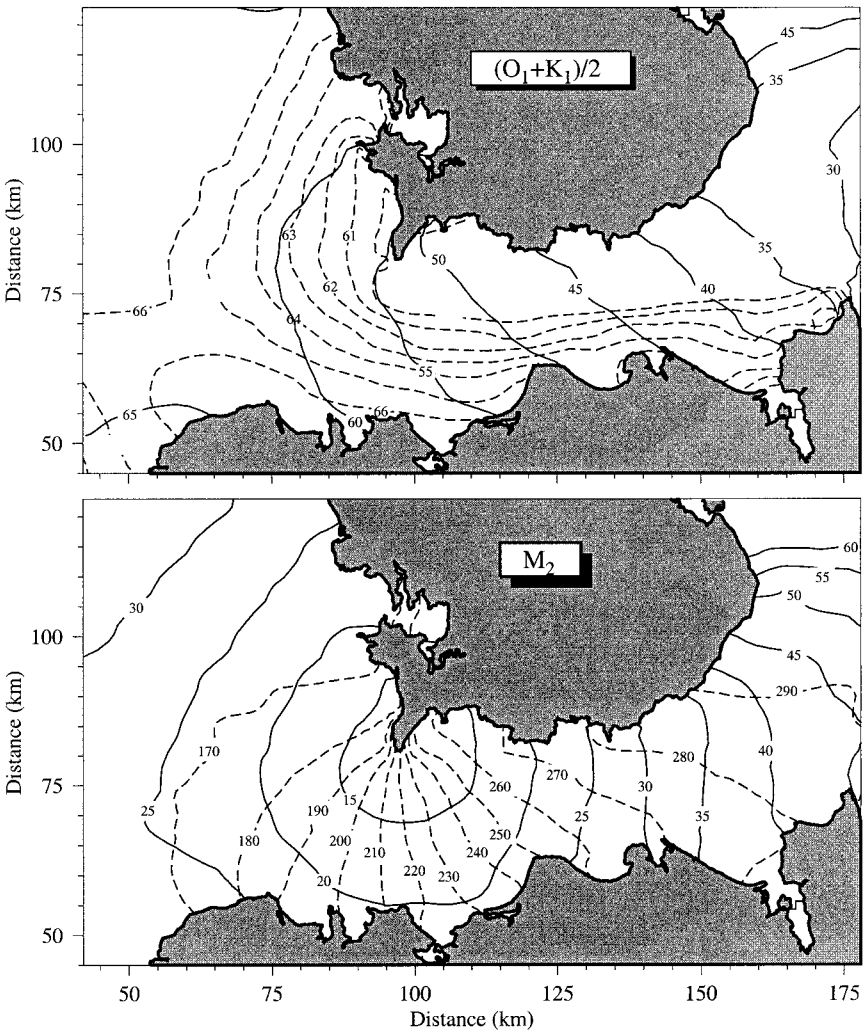

FIG. 13. Model-predicted cotidal amplitudes (solid lines) and phases (dashed lines) of diurnal ($(O_1 + K_1)/2$) and semidiurnal M_2 tidal constituents. Units: coamplitude (cm) and cophase (deg).

tidally rectified currents: either O_1 or K_1 residual current is about 10 times larger in magnitude than the M_2, tidally rectified current. The magnitude and spatial distribution of the sum of the M_2, O_1, and K_1 tide-induced residual currents is almost identical to the one shown in Fig. 14. This suggests that the interaction between semidiurnal and diurnal, as well as diurnal tides themselves, in Qiongzhou Strait is not significant.

A momentum balance analysis for the x (almost alongstrait) and y (almost cross-strait) components of the equations of motion was conducted to examine the physical processes that cause the formation of the westward flow (Fig. 15). The results show that in the alongstrait direction the bottom stress and Coriolis force terms are one order of magnitude smaller than the nonlinear advection and surface pressure gradient force terms, which means they are negligible with respect to the momentum balance. Near the northern coast, two dominant terms are the horizontal advection terms $u\partial u/\partial x$ and $v\partial u/\partial y$, while near the southern coast the dominant terms are still $u\partial u/\partial x$ and $v\partial u/\partial y$, but the vertical advective term ($w\partial u/\partial z$) and the alongstrait surface pressure gradient force ($-g\partial\zeta/\partial x$) cannot be ignored. In the cross-strait direction, the bottom stress in the strong residual flow region is still negligible compared with the cross-strait surface pressure gradient force. Near the northern coast, the westward flow is driven under the momentum balance between the cross-strait surface pressure gradient force ($-g\partial\zeta/\partial y$), the Coriolis force ($fu$), and the horizontal advective term ($v\partial v/\partial y$). Near the southern coast, two horizontal advection terms, $u\partial v/\partial x$ and $v\partial v/\partial y$, are dominant. The Coriolis force and cross-strait surface pressure gradient force cannot be ignored as first-order contributions. This suggests that the westward residual flow in the strait is driven by a strong nonlinear process in which the horizontal ad-

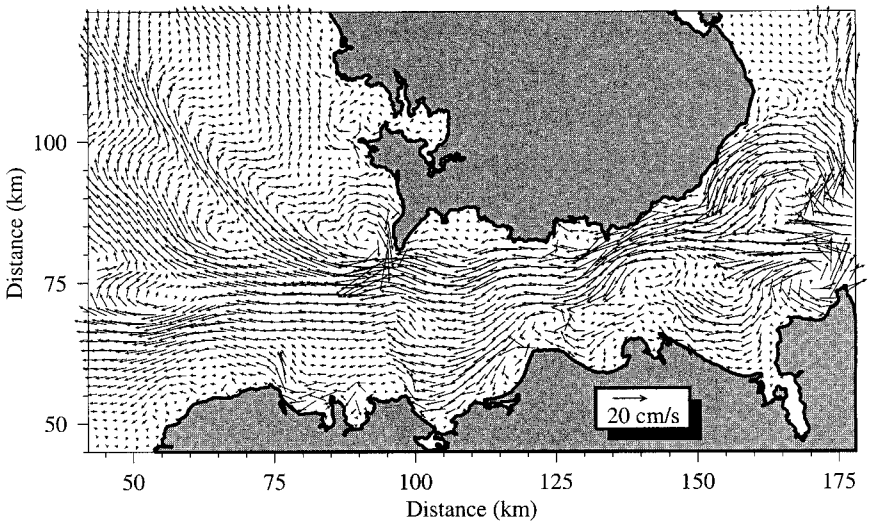

FIG. 14. Spatial distribution of the model-predicted surface residual current vectors in Qiongzhou Strait and adjacent area.

vection terms, the Coriolis force, and cross-strait surface pressure gradient force must all be taken into account.

The momentum balance analysis suggests that the strong westward residual current in Qiongzhou Strait is driven by tidal rectification associated with the complex nonlinear interaction of tidal currents over variable bottom topography. This nonlinear process is very similar to that proposed by Chen et al. (1999) in which nonlinear advections are dominant.

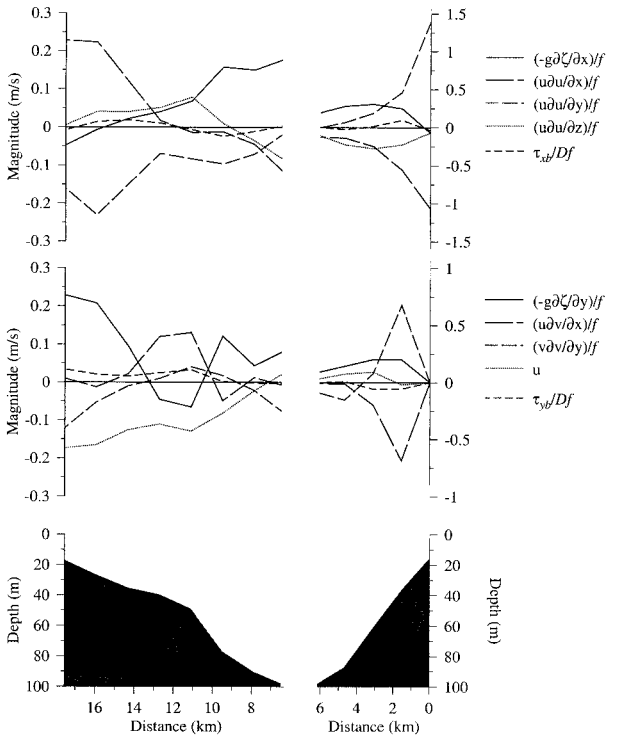

FIG. 15. Cross-strait distribution of each term in the vertically averaged *x*- (almost alongstrait) and *y*- (almost cross-strait) momentum equations.

6. Discussion

Westward mean flow through Qiongzhou Strait would directly alter the seasonal circulation in the SCS. The previous understanding of seasonal circulation in the Gulf of Beibu is based mainly on the wind-driven theory, which is cyclonic in winter and anticyclonic in summer. This seasonal circulation pattern has recently been challenged by long-term current measurements taken on the northeastern side of the Gulf of Beibu, which show a cyclonic circulation pattern also in summer (Shi and Gao 1998). Our finding in this study clearly demonstrates that the mean current in Qiongzhou Strait has a direct impact on the seasonal circulation in the Gulf of Beibu. This can be seen from a simple quantitative estimation of water transport. The area of the Gulf of Beibu is about 1.3×10^{11} m^2 and the average water depth is 46 m, which results in a total volume of about 6.0×10^{12} m^3. The westward mean flow in Qiongzhou Strait is 10–30 cm s^{-1} in summer, which accounts for a transport of 0.1–0.2 Sv into the Gulf of Beibu. Integrating the transport over a season (3 months) produces a volume of 0.8–1.6 ($\times 10^{12}$ m^3), which would occupy about 13%–27% of the total volume in the Gulf of Beibu. This suggests that the outflow of Qiongzhou Strait could be a significant contributor to the cyclonic circulation during summer in the Gulf of Beibu. If this is true, does the northward circulation along the western coast of the SCS between Vietnam and China still exist in summer? Or are there two circulation gyres in the Gulf of Beibu, an anticyclonic one in the western region

and a cyclonic one in the eastern region? These questions need to be addressed in future field measurements and modeling efforts.

Many of the previous modeling efforts in the SCS have neglected the passage of water through Qiongzhou Strait between the Gulf of Beibu and the northeastern region of the SCS due to limitations in model grid resolution. Although some recent modeling efforts have included this strait, they still fail to resolve realistic coastal circulation patterns because of the lack of tidal forcing. Ignoring the water exchange through Qiongzhou Strait would result in an unrealistic circulation pattern in the northern shelf of the SCS, and thus lead to an incorrect mass balance in this region. If Qiongzhou Strait acts like a water pump for the northeastern SCS, there should be a cyclonic or westward circulation around the northeastern coast of Hainan Island or in the northeastern SCS to compensate for water loss through the strait. Would Qiongzhou Strait have an influence only on local circulation over the continental shelf and the Gulf of Beibu or would it affect the regional circulation of the SCS? In other words, do coastal processes play an important role in seasonal variations of the SCS circulation? These questions must be taken into account in order to provide a comprehensive understanding of seasonal variations in the circulation patterns of the SCS.

It is well known that the China Sea is characterized by two cold water masses: one, called the ''Yellow Sea Cold Water'' (YSCW), forms in the East/Yellow Seas (Chen et al. 1994) and another, called the ''Beibu Gulf Cold Water'' (BGCW), forms in the Gulf of Beibu in the SCS. The YSCW is located in a midlatitude region, with significant seasonal variation in the vertical due to seasonal surface cooling/heating. This water forms in the winter due to surface cooling and mixing. It then becomes trapped on the bottom during spring and summer, isolated from the surface water by a relatively strong thermocline formed by spring/summer surface heating. In the Gulf of Beibu, however, the seasonal variation of temperature is less than 5°C. The main source of the BGCW is the cold and less saline water originating in river discharges along the northeastern coast of the SCS and the northwestern coast of the Gulf of Beibu in winter through spring. This water generally forms in March in the northern Gulf of Beibu and grows in volume from May to June. Then it moves and diffuses southward in July, and finally disappears in late August or early September—a lifetime of about 6 months. An example of the location and vertical structure of the BGCW can be viewed in Fig. 16, which shows the distribution of surface and bottom temperatures in the Gulf of Beibu. The hydrographic data used in this figure were collected during 1–30 June 1964. The year-round water input from Qiongzhou Strait would have a significant influence on the formation, evolution, and fate of the GBCW in winter through summer. It is clear that Qiongzhou Strait acts as a water passage that transports the cold and less saline coastal water into the Gulf of Beibu to form the GBCW in winter. It also tends to intensify this water in spring. However, it is still unknown whether or not the continuous outflow from Qiongzhou Strait affects the southward migration and dissipation of the GBCW and finally causes it to disappear in the Gulf of Beibu. These questions could be investigated using remote sensing of SST and regional hydrographic surveys.

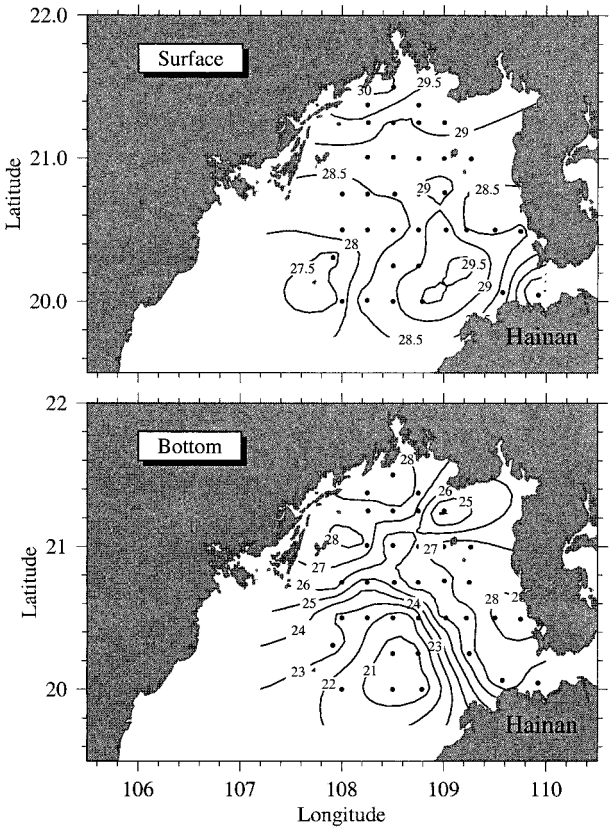

FIG. 16. Distributions of the surface and bottom temperatures in the Gulf of Beibu during the 1–30 Jun 1964 hydrographic survey. The measurement stations are indicated by dots.

Tidal-induced mixing is energetic throughout the year in Qiongzhou Strait. Mixing against seasonal surface heating would create the temperature front in the shallower region on both northern and southern coasts. Significant internal tides should be energetic over variable bottom topography across the strait, especially in summer, and the nonlinear interaction of internal and barotropic tides over variable bottom topography would directly intensify the alongstrait residual flow through stratified tidal rectification (Chen et al. 1995). Since no temperature and salinity data are available for this study, we could not further verify the intensity and structure of stratified tidal rectified flow due to internal tides in the strait. Previous temperature measurements were generally made at different times and locations in the strait. Those data fail to provide a snapshot of cross and

alongstrait distributions of temperature because of a significant diurnal variation of temperature due to land–sea interaction. We tried to make several temperature and salinity measurements across and along the strait in July 1999, but our efforts were unsuccessful due to unknown calibration errors in the CTD. Despite these problems, the previous hydrographic data reveal a remarkable cross-strait gradient of temperature year-round, and an intensification of vertical stratification in Qiongzhou Strait during the summer (Wang 1998). Future studies of the dynamics in Qiongzhou Strait should pay attention to the stratified tidal rectification due to internal tides.

7. Summary

An analysis of surface elevation and current data taken in Qiongzhou Strait over the last 37 years (1963–99) was made to examine the role of this strait in the seasonal variation of the SCS circulation. This analysis has revealed that Qiongzhou Strait is an active area of tidal wave interaction and a source region for westward water transport into the Gulf of Beibu (Gulf of Tonkin). The semidiurnal tidal wave propagates eastward from the Gulf of Beibu through Qiongzhou Strait, while diurnal tidal waves enter the strait from both the eastern and western sides. A westward mean flow of 10–40 cm s^{-1} is found through Qiongzhou Strait during all seasons, which accounts for water transports of 0.2–0.4 Sv and 0.1–0.2 Sv into the Gulf of Beibu in winter–spring and summer–autumn, respectively.

The observed mean flow in Qiongzhou Strait is in the same direction as that predicted for large-scale wind force in winter but opposes that in summer. Several numerical experiments were conducted to examine the physical mechanism responsible for the formation of the year-round westward mean flow in the strait. The model provides a reasonable simulation of semidiurnal and diurnal tidal waves through Qiongzhou Strait, and the model-predicted residual flow is in agreement with the observed mean flow. The momentum balance analysis suggests that the strong westward residual current in the strait is driven by the tidal rectification associated with the complex nonlinear interaction of tidal currents over variable bottom topography. This nonlinear process is very similar to that proposed by Chen et al. (1999) in which nonlinear advection is dominant.

The existence of the westward mean flow in Qiongzhou Strait could have a significant influence on the seasonal circulation of the SCS, especially in the Gulf of Beibu. This is probably the reason that the anticyclonic circulation disappears in the northern Gulf of Beibu during summer. Further exploration in terms of field measurements and modeling on the continental shelf of the SCS are encouraged if we are to gain a more comprehensive understanding of seasonal circulation patterns in the SCS and the various roles played by river discharge, tidal forcing, complex coastal topography, and wind forcing.

Acknowledgments. This research was supported by the U.S.–China Marine Ecosystem Modeling Laboratory, Institute of Oceanology, Chinese Academy of Sciences, People's Republic of China, under the Chinese National Sciences Foundation Grants 49928605 and 49976032 and the Georgia Sea Grant College Program under Grants NA26RG0373 and NA66RG0282. We appreciated all the efforts of anonymous Chinese scientists in collecting data over the last 37 years, and Bob Beardsley and anonymous reviewers for their valuable critical comments and constructive suggestions. Bob Beardsley and George Davidson helped edit this manuscript, and their help is greatly appreciated.

REFERENCES

Blumberg, A. F., and G. L. Mellor, 1987: A description of a three-dimensional coastal ocean circulation model. *Three Dimensional Coastal Models*, N. Heaps, Ed., *Coastal and Estuarine Sciences*, Vol. 5, Amer. Geophys. Union, 1–6.

Cao, D. M., and G. H. Fang, 1990: A numerical tidal model for the northern South China Sea. *Tropic Oceanogr.,* **9** (2), 63–67.

Casulli, V., 1990: Semi-implicit finite-difference methods for the two-dimensional shallow water equations. *J. Comput. Phys.*, **86,** 56–74.

Chao, S. Y., P. T. Shaw, and S. S. Wu, 1996: Deep water ventilation in the South China Sea. *Deep-Sea Res.*, **43,** 445–466.

Chen, C., and R. C. Beardsley, 1995: A numerical study of stratified tidal rectification over finite-amplitude banks. Part I: Symmetric bank. *J. Phys. Oceanogr.,* **25,** 2090–2110.

——, and ——, 1998: Tidal mixing and cross-frontal particle exchange over a finite amplitude asymmetric bank: A model study with application to Georges Bank. *J. Mar. Res.,* **56,** 1165–1201.

——, ——, R. Limeburner, and K. Kim, 1994: Comparison of winter and summer hydrographic observations in the Yellow and East China Seas and adjacent Kuroshio during 1986. *Cont. Shelf Res.*, **14,** 909–929.

——, ——, and ——, 1995: A numerical study of stratified tidal rectification over finite-amplitude banks. Part II: Georges Bank. *J. Phys. Oceanogr.,* **25,** 2111–2128.

——, L. Zheng, and J. Blanton, 1999: Physical processes controlling the formation, evolution, and perturbation of the low-salinity front in the inner shelf off the Southeastern U.S.: A model study. *J. Geophys. Res.,* **104,** 1259–1288.

——, R. Beardsley, and P. J. S. Franks, 2001: A 3-D prognostic numerical model study of the Georges Bank ecosystem. Part I: Physical model. *Deep-Sea Res. II,* **48,** 419–456.

Chu, P. C., S. Lu, and Y. Chen, 1997: Temporal and spatial variability of the South China Sea surface temperature anomaly. *J. Geophys. Res.,* **102,** 20 937–20 955.

——, Y. Chen, and S. Lu, 1998: Wind-driven South China Sea deep basin warm-core/cool-core eddies. *J. Oceanogr.,* **54,** 347–360.

Ding, W. L., 1986: The characteristics of the distribution of tidal elevation and currents in the South China Sea (in Chinese). *J. Oceanogr. Limnol.,* **17** (6), 468–480.

Foreman, M. G. G., 1978: Manual for tidal analysis and prediction. Pacific Marine Science Rep. 78-6, Institute of Ocean Sciences, Patricia Bay, Sydney, British Columbia, Canada, 70 pp.

Huang, Q. Z., W. W. Li, and Y. S. Li, 1994: Current characteristics of the South China Sea (in Chinese). *Oceanogr. China Seas,* **1,** 39–47.

Liu, Z., H. Yang, and Q. Liu, 2001: Regional dynamics of seasonal

variability in the South China Sea. *J. Phys. Oceanogr.,* **31,** 272–284.

Loder, J. W., 1980: Topographic rectification of tidal current on the sides of Georges Bank. *J. Phys. Oceanogr.,* **10,** 1399–1416.

Metzger, E. J., and H. E. Hurlburt, 1996: Coupled dynamics of the South China Sea, the Sulu Sea, and the Pacific Ocean. *J. Geophys. Res.,* **101** (C5), 12 331–12 352.

Pohlmann, T., 1987: A three-dimensional circulation model of the South China Sea. *Three-Dimensional Models of Marine and Estuarine Dynamics,* J. C. J. Nihoul and B. M. Jamart, Eds., Elsevier, 245–268.

Shaw, P. T., and S. Y. Chao, 1994: Surface circulation in the South China Sea. *Deep-Sea Res.,* **41,** 1663–1683.

——, ——, K. K. Liu, S. C. Pai, and C. T. Liu, 1996: Winter upwelling off Luzon in the northeastern South China Sea. *J. Geophys. Res.,* **101,** 16 435–16 448.

——, ——, and L. Fu, 1999: Sea surface height variations in the South China Sea from satellite altimetry. *Oceanol. Acta,* **22,** 1–17.

Shi, M., and G. Gao, 1998: Analysis of the long-term current meter measurement data in the Gulf of Beibu and around the Weizhou Island (in Chinese). Report of the hydrographic and meteorological observational data analysis in the Gulf of Beibu and around the Weizhou Island, Ocean University of Qingdao, 230 pp.

Wang, L., 1998: Study on Qiongzhou Strait water exchange and its dynamic mechanism (in Chinese). Chinese National Sciences Foundation Tech. Rep. 49566011, 227 pp.

Wyrtki, K., 1961: Physical Oceanography of the Southeast Asian waters. NAGA Report 2, Scientific results of marine investigations of the South China Sea and the Gulf of Thailand. Scripps Institution of Oceanography, La Jolla, CA, 195 pp.

Yu, M. G., and J. F. Liu, 1993: The system and pattern of the South China Sea circulation (in Chinese). *Ocean Predict.,* **10** (2), 13–17.